Monte Carlo Simulations of Electrons in Al_4SiC_4 Ternary Carbide

K. Kalna[1] and D. Chaussende[2]

[1] NanoDeCo Group, Dept. Electronic & Electrical Engineering, Faculty of Science & Engineering, Swansea University, Swansea, SA1 8EN, Wales, United Kingdom

[2] Université Grenoble Alpes, CNRS, Grenoble INP, SIMaP, 38000 Grenoble, France

Email: k.kalna@swansea.ac.uk

An Al_4SiC_4 ternary carbide has become a promising wide band-gap semiconductor for the semiconductor industry over the last decade because of its emerging properties [1]. A crystal structure of Al_4SiC_4 is illustrated in Fig. 1. The Al_4SiC_4 band-gap has been calculated to be 2.48 eV [2,3] thus opening a possibility for the design of carbide heterostructure devices in a combination with 4H-SiC or 3C-SiC. These heterostructure carbide devices could potentially resolve issues with the large interface density of states at the semiconductor interface with a dielectric layer leading to a low inversion carrier mobility in SiC MOSFETs [4]. Other remarkable properties include superior oxidation resistance [5], superior wear resistance, low weight, high strength, and high thermal conductivity [6].

In this work, an ensemble Monte Carlo (MC) simulation code is developed to investigate the electron transport in bulk Al_4SiC_4. Al_4SiC_4 has a wurzite lattice [2,3] as shown in Fig. 2. We assume that the two lowest valleys will play a role in electron transport. The M-valley has also six locations contributing one-half (a total of 3 equivalent valleys). The K-valley has six locations contributing one-third to the 1st Brillouin zone (a total of 2) as shown in Figs. 3 ad 4. Therefore, a two-valley non-parabolic anisotropic bandstructure model is employed with the M-valley to be a minimum and the second K-valley to be 0.52 eV above as illustrated in Fig. 5. The electron interactions with polar and non-polar phonons within and between M- and K-valleys are listed in Table 1. The material parameters in Table 2 use a mix of experimental and theoretical sources like optical phonon energies extracted from IR/Raman spectroscopy [3].

Valley	Transition	Scattering Type
M_1	$M_1 \to M_1$	Intra Polar
	$M_1 \to M_{2,3}$	Inter Non-Polar
	$M_1 \to K$	Inter Non-Polar
M_2	$M_2 \to M_2$	Intra Polar
	$M_2 \to M_{1,3}$	Inter Non-Polar
	$M_2 \to K$	Inter Non-Polar
M_3	$M_3 \to M_3$	Intra Polar
	$M_3 \to M_{1,2}$	Inter Non-Polar
	$M_3 \to K$	Inter Non-Polar
K	$K \to M_1$	Inter Non-Polar
	$K \to M_2$	Inter Non-Polar
	$K \to M_3$	Inter Non-Polar

Table 1: Electron-phonon scattering transitions considered in the MC model.

Finally, M-valley **k**-vector (inverse) transformations to a spherical space (denoted by *) within the anisotropic analytical model use a combination of Herring-Vogt and rotational transformations [8] as:

Table 2: Al_4SiC_4 material parameters considered in the MC simulations.

Parameter [Unit]	Value
Mass Density [g/cm^3]	3.03 [a]
Lattice Const. [Å]	3.28 [a]
Piezoelectric Const. [C/m^2]	0.47 [a]
Longitudinal Acoustic Velo. [m/s]	10577 [a]
Transverse Acoustic Velo. [m/s]	6431 [a]
Polar Opt. Phon. Energy [meV]	67.32 [b], 107.24 [b]
Non-Polar Opt. Phon. Energy [meV]	85.55 [b]
Acoustic Def. Potential [eV]	11.4 [c]
Indirect Band Gap for the M-valley	$E_G^{(M)} = 2.78$
(M) & the K-valley (K) [eV]	$E_G^{(K)} = 3.30$ [a]
Electron Effective Masses [m_e]	$m_l^{*(M)} = 0.568$ [d]
	$m_t^{*(M)} = 0.695$ [d]
	$m_l^{*(K)} = 1.057$ [d]
	$m_t^{*(K)} = 0.936$ [d]

[a]Ref. [2]. [b]Ref. [3]. [c]Average taken from [7]. [d]Extracted value from DFT calculations [2]. m_e is the rest mass of an electron.

$$k_x^*(k_x) = k_x(k_x^*)cos(\theta) - (+)k_y(k_x^*)sin(\theta) \quad (1)$$

$$k_y^*(k_y) = k_y(k_y^*)cos(\theta) + (-)k_x(k_y^*)sin(\theta) \quad (2)$$

$$k_z^*(k_z) = k_z(k_z^*) \quad (3)$$

The MC simulations in Figs. 6 and 7 predict that Al_4SiC_4 will have a maximum electron drift velocity of 1.35×10^7 cms^{-1} at an electric field of 1400 kVcm^{-1} and a maximum electron mobility of 82.9 cm^{2}V^{-1}s^{-1}. Fig. 8 shows the electron mobility dependence on ionized impurity concentration. The average electron kinetic energy and valley occupation are plotted in Figs. 9 and 10, respectively.

References

[1] T. Liao, J. Y. Wang, and Y. C. Zhou, *Phy. Rev.* B **74** (17), 1098-1121 (2006).

[2] L. Pedesseau et al., *APL Materials* **3** (12), 121101 (2015).

[3] D. Zevgitis et al., *Synthesis and Characterization of Al_4SiC_4: A "New" Wide Band Gap Semiconductor Material*, *Materials Science Forum* 821-823, 974-977 (2015).

[4] S. Forster, D. Chaussende, and K. Kalna, *ACS Appl. Energy Mater.* **2** (9), 3001-3007 (2020).

[5] K. Inoue and A. Yamaguchi, *J. Am. Ceram. Soc.* **86** (6), 1028-1030 (2003).

[6] W. Y. Ching, and P. Rulis, *Electronic Structure Methods for Complex Materials: The Orthogonalized Linear Combination of Atomic Orbitals*, OUP Oxford, 2012.

[7] H. Iwata and K. M. Itoh, *J. Appl. Phys.* **89** (11), 6228-6234 (2001).

[8] S. Forster, D. Chaussende, and K. Kalna, *ACS Appl. Energy Mater.* **2** (1), 715-720 (2019).

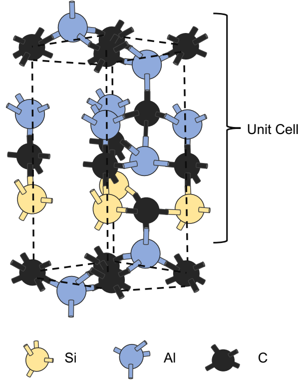

Fig. 1: A crystal structure of Al_4SiC_4. The blue, yellow, and black spheres represent Al, Si, and C atoms, respectively.

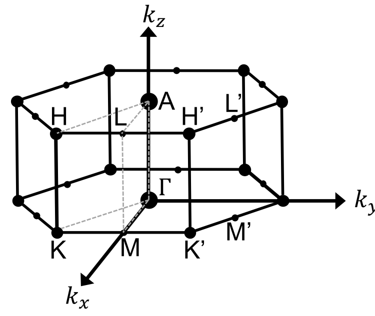

Fig. 2: A schematic of hexagonal bandstructure of Al_4SiC_4 in the **k**-space showing a location of principal valleys.

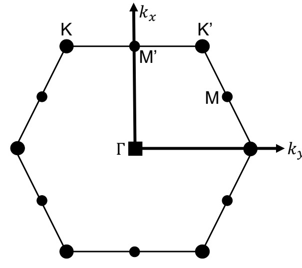

Fig. 3: The hexagonal (0001) $\mathbf{k_x} - \mathbf{k_y}$ plane of Al_4SiC_4 showing a location of principal valleys.

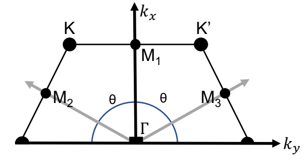

Fig. 4: Detail of locations of the M-valleys in the (0001) plane within the Al_4SiC_4 hexagonal structure, where $\theta = \pm 60^\circ$ or $\pi/3$.

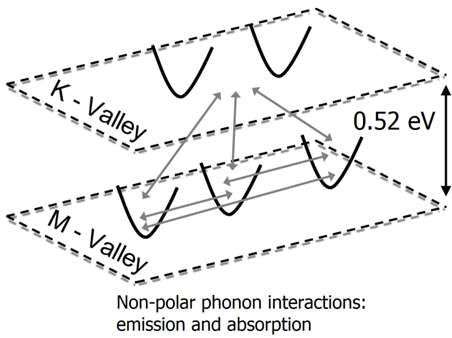

Fig. 5: A schematic of conduction band minimum valleys for Al_4SiC_4 showing details of the number of equivalent M- and K- valleys, the separation between valleys, and the electron—non-polar phonon interactions considered in the transport model.

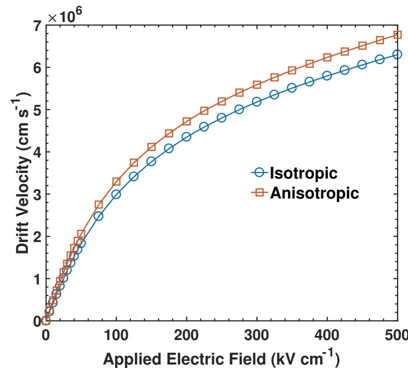

Fig. 6: Electron drift velocity as a function of applied electric field in a bulk Al_4SiC_4. The velocity obtained assuming an anisotropic (red squares) and a simpler isotropic (blue circles) bandstructure are shown.

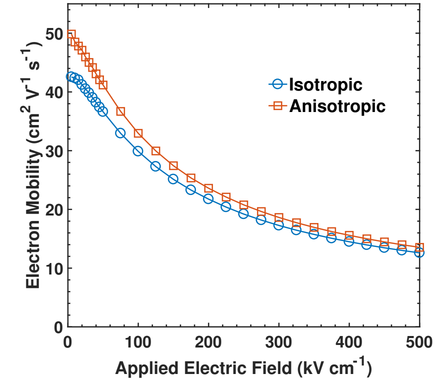

Fig. 7: Electron mobility as a function of applied electric field in a bulk Al_4SiC_4. The mobility obtained assuming an anisotropic (red squares) and a simpler isotropic (blue circles) bandstructure are plotted.

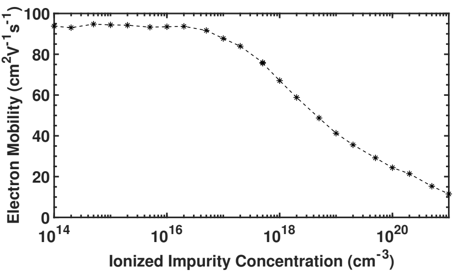

Fig. 8: Electron mobility as a function of ionized impurity concentration in a bulk Al_4SiC_4.

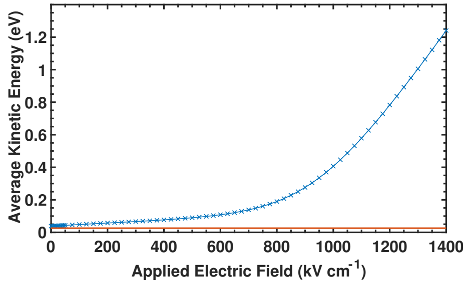

Fig. 9: Average kinetic energy as a function of applied electric field in a bulk Al_4SiC_4.

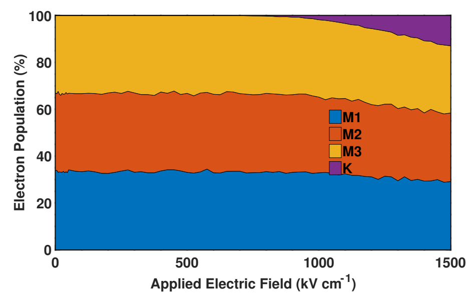

Fig. 10: Valley occupancy of electrons in the M- and K-valleys vs. applied electric field in bulk Al_4SiC_4.